land

MDPI

Article

Effects of Green–Gray–Blue Infrastructure Adjustments on Urban Drainage Performance: Time Lag and H–Q Curve Regulation

Yang Yu [1], Yi Yao [2,*], Chentao Li [3] and Dayang Li [4,5]

[1] School of Environment, Tsinghua University, Beijing 100084, China
[2] The National Key Laboratory of Water Disaster Prevention, Nanjing Hydraulic Research Institute, Nanjing 210029, China
[3] The National Key Laboratory of Water Disaster Prevention, Hohai University, Nanjing 210098, China
[4] School of Civil Engineering, Yancheng Institute of Technology, Yancheng 224051, China
[5] School of Geography and Ocean Science, Nanjing University, Nanjing 210023, China
* Correspondence: yiyao@nhri.cn

Abstract: With the increasing frequency of extreme rainfall events, enhancing urban drainage systems' regulation capacity is crucial for mitigating urban flooding. Existing studies primarily analyze infrastructure impacts on peak flow delay but often lack a systematic exploration of time-lag mechanisms. This study introduces the time-lag parameter, using the hysteresis curve of the water level–flow rate relationship to quantify drainage system dynamics. An SWMM-based drainage model was developed for the Rongdong area of Xiong'an New District to evaluate the independent roles of green, gray, and blue infrastructures in peak flow reduction and time-lag modulation. The results indicate that green infrastructure extends the horizontal width and reduces the vertical height of the hysteresis curve, prolonging time lag and making it effective for small-to-medium rainfall. Gray infrastructure enhances drainage efficiency by compressing the hysteresis curve horizontally and increasing its vertical height, facilitating rapid drainage but offering limited peak reduction. Blue infrastructure, by lowering outlet water levels, improves drainage capacity and reduces time lag, demonstrating adaptability across various rainfall scenarios. This study systematically quantifies the role of each infrastructure type in time-lag regulation and proposes a collaborative optimization strategy for urban drainage system design.

Keywords: urban drainage system; hysteresis curve; time-lag effect; infrastructure optimization

check for updates

Academic Editor: Fabio Luino

Received: 8 January 2025
Revised: 4 February 2025
Accepted: 15 February 2025
Published: 17 February 2025

Citation: Yu, Y.; Yao, Y.; Li, C.; Li, D. Effects of Green–Gray–Blue Infrastructure Adjustments on Urban Drainage Performance: Time Lag and H–Q Curve Regulation. *Land* **2025**, *14*, 419. https://doi.org/10.3390/land14020419

Copyright: © 2025 by the authors. Licensee MDPI, Basel, Switzerland. This article is an open access article distributed under the terms and conditions of the Creative Commons Attribution (CC BY) license (https://creativecommons.org/licenses/by/4.0/).

1. Introduction

The frequency and intensity of extreme rainfall events have significantly increased with global climate change, posing escalating challenges to urban drainage systems [1,2]. In the process of urbanization, low-lying areas face reduced natural infiltration capacity and expanded hardened surfaces, which diminish the performance of traditional drainage systems under high-intensity rainfall, a situation compounded by changing rainfall patterns, exacerbating urban flooding issues [3–5]. Although peak flow reduction and waterlogging control have alleviated flooding to some extent, the insufficient dynamic response capacity of urban drainage systems remains a major bottleneck that urgently requires optimization.

Existing research has extensively examined urban drainage system optimization, primarily focusing on static performance metrics such as peak flow reduction, waterlogging control, and structural design improvements. Previous studies have demonstrated that green infrastructure (e.g., rain gardens and sunken green spaces) can effectively reduce runoff and

delay peak flow arrival during small-to-medium rainfall events [6–8]; gray infrastructure (e.g., drainage networks) significantly enhances drainage capacity through structural optimization [9,10]; and blue infrastructure (e.g., wetlands and lakes) leverages natural retention functions to alleviate downstream drainage pressure [11,12]. Recent research has also explored the combined benefits of hybrid blue–green–gray solutions, emphasizing their role in achieving integrated flood risk reduction and system resilience. These findings highlight that green, blue, and gray infrastructures contribute to peak flow reduction and peak delay.

However, existing studies predominantly focus on the static impacts of facilities in delaying peak flow timing, often confined to specific rainfall scenarios. There remains a lack of systematic and mechanistic exploration into the dynamic processes underlying lag effects, particularly in terms of how different infrastructure types interact with drainage system hydrodynamics. Time lag, a critical dynamic indicator describing the propagation delay of peak flow from catchment areas to drainage outlets [13,14], provides a comprehensive reflection of the dynamic changes in the drainage process [15]. It encompasses the entire process from rainfall onset to water collection and discharge. The length of the time lag directly influences the system's capacity to mitigate rainfall impacts: a longer lag can effectively alleviate the instantaneous pressure of short-duration intense rainfall on drainage facilities, while a shorter lag may exacerbate drainage bottlenecks [13].

Traditional studies have largely overlooked the explicit role of time lag in drainage network performance, concentrating primarily on peak timing delays without fully considering the interdependencies between time-lag variation, infrastructure function, and system resilience. Recent advances in hydrological modeling and flood risk management suggest that a more dynamic perspective is required to assess the effectiveness of infrastructure adaptations in mitigating urban flooding challenges [16,17].

To address these issues, this study conducts an in-depth investigation into the dynamic characteristics of time lag, focusing on its behavior and mechanisms under the influence of different types of infrastructure. Green infrastructure's source control function, gray infrastructure's enhanced drainage efficiency, and blue infrastructure's natural retention capacity collectively form key factors affecting time lag. By analyzing the regulatory roles of these three types of infrastructure in water dynamics, this study explores their potential impacts on time-lag characteristics and the morphology of the water level–flow rate relationship curve (H–Q curve), uncovering the intrinsic link between infrastructure types and time-lag variation.

Using the Rongdong area of Xiong'an New District as the study area, this research constructs an SWMM-based drainage network model to systematically analyze the independent effects and dynamic characteristics of green, gray, and blue infrastructures on time lag in urban drainage systems. The specific research objectives are as follows: (1) To construct a dynamic response model of the drainage system under extreme rainfall conditions and analyze the full evolution of the water level–flow rate relationship. (2) To quantitatively evaluate the independent effects of green, gray, and blue infrastructures on time lag and uncover their regulatory mechanisms. (3) To explore effective pathways for optimizing system dynamic responses through facility design parameters. The novelty of this study lies in quantitatively assessing the independent impacts of the three types of infrastructure on time lag and H–Q curve morphology from both dynamic and mechanistic perspectives. By filling the gaps in existing research, this work provides scientific insights for optimizing urban drainage system design and improving resilience to extreme rainfall.

2. Material and Methods

2.1. Study Area

This study focuses on the Rongdong area of Xiong'an New District, a low-lying region in the North China Plain and one of the core areas for development in Xiong'an New

District [18,19]. The area spans approximately 32.5 km^2 and is geographically located between 38°39′ and 38°44′ N latitude and 116°0′ and 116°5′ E longitude [20] (Figure 1a). The topography of Rongdong is flat, with an average elevation ranging from 6.5 to 7.5 m, gradually sloping from northwest to southeast, and is characterized by typical low-lying plains. The region boasts a developed network of rivers and lakes, including significant waterways such as the Baigou River and Daqing River, as well as multiple wetlands and lakes. This interconnected hydrological system is linked to Baiyangdian Lake, the largest freshwater lake in North China, which plays a crucial role in regional drainage regulation. However, seasonal fluctuations in Baiyangdian's water level during flood periods may impose constraints on the drainage system.

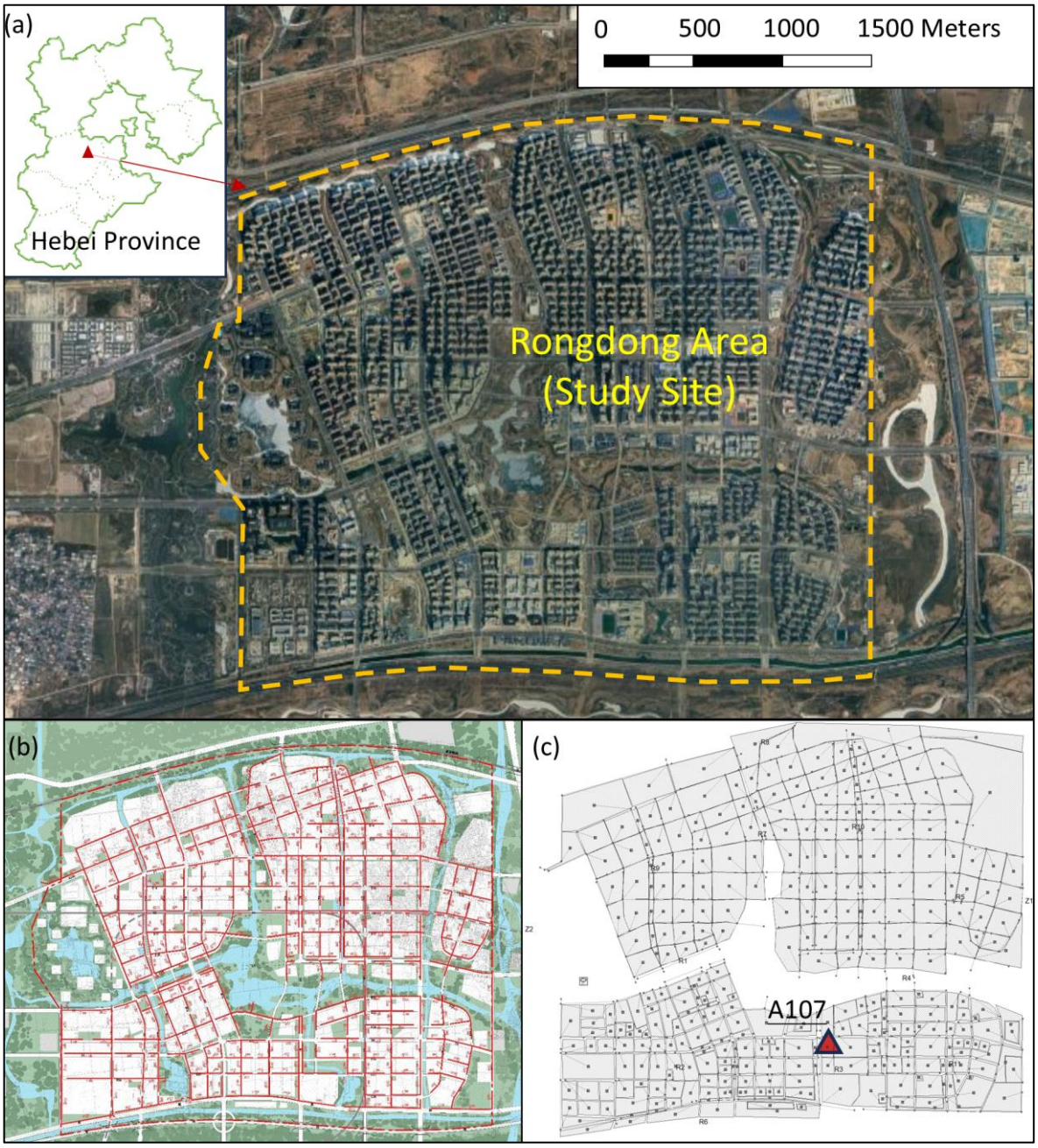

Figure 1. Geographic location and drainage system planning of the Rongdong area. (**a**) Geographic location of the Rongdong area; (**b**) schematic diagram of drainage system planning; (**c**) layout of the SWMM model.

The Rongdong area falls under a temperate semi-arid continental monsoon climate zone, with an average annual precipitation of 522.9 mm, over 80% of which occurs during the flood season from June to September [21]. Frequent extreme rainfall events in the region often lead to concentrated storm runoff, exacerbating the propagation delay of flood peaks and significantly increasing the instantaneous load on drainage systems, thereby heightening the risk of urban flooding [22]. During heavy rainstorms, the existing drainage system often lacks sufficient retention capacity and dynamic response capability to effectively mitigate the pressure on pipelines and rivers caused by peak flows.

To address these challenges, a multi-level rainwater drainage network has been planned for the Rongdong area, considering its unique topographical and hydrological characteristics (Figure 1b). In the Rongdong area, rainwater is collected through a structured underground drainage network and discharged into surrounding rivers or retention facilities via pumping stations. The system follows a separated sewer system, ensuring the effective management of stormwater and wastewater. The total pipeline network spans over 150 km, with pipe diameters ranging from 600 mm to 2200 mm and burial depths varying from 1.5 m to 9.0 m. To enhance flood resilience, the area incorporates multiple initial rainwater retention tanks with capacities ranging from 2000 m^3 to 6500 m^3. Major waterways, such as the Nanjuma River and the Baigou Diversion River, serve as key conduits for runoff collection and flood discharge, supported by pumping stations and flood retention facilities to alleviate drainage pressure during storms. However, despite the initial establishment of the drainage planning framework, the area continues to face challenges such as insufficient localized drainage capacity and flood risks under extreme rainfall conditions [23,24].

2.2. SWMM Model

2.2.1. Model Construction

This study employs the SWMM 5.2 model to construct a one-dimensional drainage network for simulating runoff and the dynamic response of the drainage system in the Rongdong area under various rainfall intensities (Figure 1c). The model integrates functional modules for green, gray, and blue infrastructures, aiming to evaluate their independent effects on peak flow reduction, waterlogging control, and drainage efficiency, thereby providing data support for optimizing urban drainage systems.

The green infrastructure module includes rain gardens, sunken green spaces, and permeable pavements, playing a critical role in source runoff control by reducing runoff volume, delaying peak flow arrival, and enhancing rainwater infiltration. The gray infrastructure module comprises drainage networks, pumping stations, and retention basins, covering main and secondary pipelines and focusing on improving drainage efficiency and rapid water evacuation. The blue infrastructure module is implemented in SWMM 5.2 by simulating dynamic water level variations in regional rivers, retention basins, and connected hydraulic structures. This module incorporates boundary conditions that reflect real-time water level fluctuations at river outlets and retention facilities, allowing for a more realistic representation of water exchange processes. In the model, retention basins are represented as storage nodes with predefined depth–storage relationships, ensuring an accurate simulation of peak flow retention and discharge regulation. Additionally, weir and outlet controls are included to mimic controlled releases from blue infrastructure, thereby alleviating downstream drainage pressure. The simulation also accounts for the influence of terrain slope, land-use distribution, and surface roughness in order to capture detailed hydrodynamic behaviors within the system.

2.2.2. Data Collection and Processing

The model inputs were sourced from planning data, field observations, and the literature, encompassing key parameters such as meteorological, topographic, and hydrological data. Meteorological data were obtained from local meteorological stations, including hourly and sub-hourly rainfall records. These data were supplemented by historical storm records to ensure that the model accounts for varying rainfall intensities. The rainfall input was derived from regional intensity–duration–frequency (IDF) curves, ensuring consistency with observed precipitation patterns. This approach enables the model to realistically simulate different storm events and their impact on urban drainage performance [25,26].

Topographic data were extracted from high-resolution digital elevation models (DEMs) with a 5 m spatial resolution, which were processed using GIS-based terrain analysis. This allowed for the accurate delineation of watershed boundaries, drainage pathways, and overland flow characteristics. The topographic dataset was integrated with the spatial distribution of both natural water bodies and constructed drainage infrastructure, ensuring that the model accurately represents flow routing across the urban landscape. By incorporating detailed terrain attributes, the model effectively captures the interactions between surface runoff and subsurface drainage networks [27]. Hydrological parameters, including pipe diameters, pumping station characteristics, and impervious surface ratios, were further calibrated through field surveys and literature comparison.

To enhance the reliability of the simulations, the model was configured with detailed specifications tailored to the study area. The simulation operates on an event-based approach, where each storm event is simulated at a 1 min time step to capture rapid hydrological responses. Each event is simulated for a total duration of up to 48 h, allowing the model to assess both immediate runoff dynamics and post-event drainage processes. The dynamic wave routing method was applied to represent unsteady flow conditions accurately and to ensure the proper simulation of backwater effects and flow attenuation within the drainage system.

The drainage network was discretized into 78 sub-catchments, each characterized by specific land-use attributes and runoff coefficients. The hydraulic network consists of 112 pipe segments, 78 junction nodes, 5 pumping stations, and 3 major retention basins. Pipe diameters range from 0.5 m to 2.5 m, with Manning's roughness coefficients assigned based on material specifications and field measurements. The boundary conditions were defined using observed river stage variations, ensuring that outflow interactions with natural water bodies were realistically represented.

2.2.3. Simulation Scenario Design

To comprehensively assess the roles of green, gray, and blue infrastructures in urban drainage systems, various simulation scenarios were designed (Table 1). The baseline scenario (GCR) reflects the current operating conditions of the drainage system and serves as a benchmark for evaluating the optimization effects of infrastructure.

The green infrastructure scenarios (G1 and G2) adjust impervious surface ratios (IAR) to simulate the effects of varying green infrastructure coverage on peak flow reduction and lag modulation. The selected impervious surface ratios (40% and 65%) represent typical urban development conditions, where lower imperviousness corresponds to well-vegetated areas with extensive green infrastructure, while higher imperviousness represents areas with intensive urbanization and limited green space. These scenarios aim to quantify the impact of surface permeability on runoff generation, infiltration, and peak flow attenuation.

The gray infrastructure scenarios (H1 and H2) modify the pipe diameters within the drainage network to analyze their impact on drainage capacity. The selected diameters (0.5 m and 1.5 m) reflect variations in pipe sizing commonly found in urban drainage

systems, where smaller diameters represent older, capacity-limited pipelines, and larger diameters simulate upgraded networks designed for enhanced flow conveyance. The modification applies to the main conduit segments within the drainage system, while secondary and tertiary pipelines maintain their existing dimensions. This ensures that the analysis reflects realistic infrastructure upgrade strategies rather than a uniform pipe size change across the entire network.

Table 1. Parameter settings for simulation scenarios.

Scenario Code	Impervious Area Ratio	Averaged Pipe Diameter (m)	Outlet Water Level During Flood Season (m)	Scenario Type
GCR	0.51	1.0	7.5	Baseline
G1	0.65	1.0	7.5	Green Infrastructure
G2	0.40	1.0	7.5	Green Infrastructure
H1	0.51	0.5	7.5	Gray Infrastructure
H2	0.51	1.5	7.5	Gray Infrastructure
B1	0.51	1.0	7.0	Blue Infrastructure
B2	0.51	1.0	6.5	Blue Infrastructure

Note: GCR = general condition reference, serving as the baseline condition for comparison.

The blue infrastructure scenarios (B1 and B2) simulate the impact of controlled water level management at drainage outlets by lowering the outlet water levels to explore the optimization effects of blue infrastructure on peak flow retention and waterlogging risk reduction. The selected outlet water levels (6.5 m and 7.0 m) align with observed fluctuations in regional river water levels during flood seasons. In practice, these modifications are achieved by adjusting the operational settings of sluice gates and pumping stations to regulate the drainage system's connectivity with receiving water bodies. This scenario reflects potential flood management strategies, where modifying downstream water levels influences upstream flow retention and drainage efficiency.

Each simulation scenario was tested under multiple rainfall conditions to assess its performance across varying storm intensities. The model was subjected to rainfall events with return periods of 5, 10, 50, 100, 200, and 1000 years, representing a range from frequent low-intensity storms to extreme rainfall events. These return periods were selected based on regional rainfall intensity–duration–frequency (IDF) curves to ensure alignment with real-world hydrological conditions. By systematically varying both infrastructure parameters and precipitation intensities, the study evaluates how different drainage configurations perform under diverse hydrological stressors.

2.2.4. Model Calibration and Validation

Two observed storm events were selected for model calibration and validation to ensure the SWMM 5.2 model accurately represents the runoff processes and operational performance of the drainage system in the study area. The calibration period utilized data from the storm event that occurred between 7 May and 9 May 2022, with model parameters adjusted to achieve optimal agreement between simulated and observed results. The validation period used data from the storm event on 4 August and 5 August 2022, employing the calibrated parameters to evaluate the model's applicability and robustness.

The selection of model parameters was based on the actual conditions and empirical values of the study area (Table 2). These parameters were fine-tuned during calibration to optimize simulation results. Key parameters for sub-catchments included slope (extracted from DEM, ranging from 0.11% to 4.67%), sub-catchment width (calculated using empirical formulas), imperviousness (determined by land-use types), Manning's roughness coefficients for previous and impervious areas (initial values of 0.8 $s \cdot m^{-1/3}$ and 0.03 $s \cdot m^{-1/3}$,

respectively), and storage depths for pervious and impervious areas (ranging from 1.27 mm to 3.50 mm). For infiltration, the Horton infiltration model was applied, adjusting the maximum and minimum infiltration rates, decay constant, and drying time to reflect regional soil characteristics. In the drainage network, the pipe roughness coefficient was set to an initial value of 0.013 and further refined based on observed results to enhance the accuracy of the drainage capacity simulation.

Table 2. SWMM model parameter calibration results.

Type	Parameter	Initial Value	Calibrated Value
Sub-Catchment	Impervious Manning's coefficient (N-Imperv)	0.03	0.03
	Pervious Manning's coefficient (N-Perv)	0.80	0.75
	Impervious storage depth (Dstore-Imperv, mm)	1.27	1.50
	Pervious storage depth (Dstore-Perv, mm)	3.18	3.50
Infiltration	Maximum infiltration rate (mm/h)	3.0	3.0
	Minimum infiltration rate (mm/h)	0.5	0.5
	Decay constant (1/h)	4.0	4.0
	Drying time (d)	7.0	7.0
Drainage	Pipe roughness	0.013	0.013

The calibration and validation results are presented in Figure 2. During critical peak flow periods, the simulated values closely matched the observed data, with only minor deviations in some instances, which may be attributed to the complexity of localized flow conditions within the network. Model performance was evaluated using the Nash–Sutcliffe Efficiency (NSE) coefficient, calculated as follows:

$$NSE = 1 - \frac{\sum_{i=1}^{N} (P_i - O_i)^2}{\sum_{i=1}^{N} (O_i - \overline{O})^2} \quad (1)$$

where P_i and O_i represent the predicted and observed values for the i-th sample, $\overline{O}$ is the mean of the observed values, and N is the total number of samples. In this study, the NSE values for the calibration and validation periods were 0.89 and 0.82, respectively, indicating that the SWMM 5.2 model has high precision and stability in capturing the dynamic characteristics of rainfall-runoff processes.

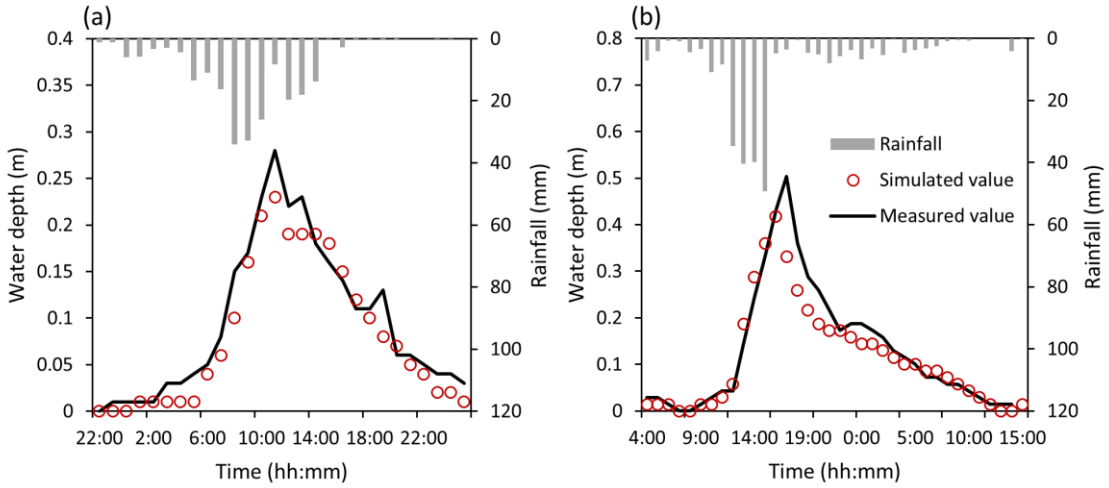

Figure 2. Comparison of observed and simulated water depths with rainfall hyetographs for calibration and validation periods at point A107. (**a**) Calibration period (7 May–9 May 2022); (**b**) Validation period (4 August–5 August 2022).

2.3. Time-Lag Analysis

Time lag, caused by storage effects, propagation delays, and hydraulic resistance, directly impacts drainage system efficiency and flood mitigation capacity [13,28]. To characterize the time-lag effect and its impact on system performance, this study employs the hysteresis curve (H–Q curve) analysis method [13,29]. The hysteresis curve area serves as a metric for retention capacity, with a larger area indicating stronger lag effects. Additionally, to systematically evaluate the independent effects of green, gray, and blue infrastructures, this study applies a comparative scenario-based approach. Each infrastructure type is assessed by isolating its influence through different simulation scenarios, allowing for the quantification of their respective impacts on time lag. Green infrastructure is analyzed based on variations in impervious surface ratios, gray infrastructure through changes in pipe diameters, and blue infrastructure by modifying outlet water levels. The impact of each type of infrastructure is quantified by comparing changes in the hysteresis curve area and lag coefficients across scenarios. This enables a structured assessment of how different infrastructure configurations influence the dynamic response of the urban drainage system.

(1) Normalization

To eliminate differences in data scales between scenarios, the time-series data were normalized using a min–max method:

$$H_{norm}(t) = \frac{H(t) - H_{min}}{H_{max} - H_{min}} \quad (2)$$

$$Q_{norm}(t) = \frac{Q(t) - Q_{min}}{Q_{max} - Q_{min}} \quad (3)$$

where $H_{norm}(t)$ and $Q_{norm}(t)$ represent the normalized water level and flow rate at time t; $H(t)$ and $Q(t)$ are the original water level and flow rate; H_{min} and Q_{min} are the minimum values; and H_{max} and Q_{max} are the maximum values. After normalization, the water level and flow rate data from different scenarios can be compared on the same scale.

(2) Calculation of Lag Coefficient

The lag coefficient is determined by the area (A) of the hysteresis curve, calculated using the following formula [13,30]:

$$A = \int_{T_1}^{T_2} |H_{norm}(t) Q_{norm}(t)| dt \quad (4)$$

where T_1 and T_2 denote the start and end times of the time interval. The curve area (A) reflects the time-lag effect between water level and flow rate: larger areas indicate more pronounced lag effects and stronger retention capacity, while smaller areas suggest more synchronous changes and faster system response.

Figure 3 illustrates typical time-lag effects between water level and flow rate, presented as a hysteresis curve and a time-series comparison. In Figure 3a, the hysteresis curve forms a closed loop, directly demonstrating the lag of flow rate (Q) behind water level (H). At the onset of rainfall, water level rises rapidly due to accumulation, whereas flow rate increases more gradually due to propagation delays and network regulation, resulting in an upward phase curve biased toward the water level axis. After rainfall ceases, water level begins to decline, while flow rate decreases at a slower rate due to the continued discharge of stored water in the network. The peak water level (H_{max}) significantly precedes the peak flow rate (Q_{max}), indicating that flow rate development and propagation are influenced by retention and frictional resistance. The time difference between the water level and flow rate peaks directly represents the time-lag effect, which is influenced by a combination of factors, including network length, gradient, pipe characteristics, and system retention capacity.

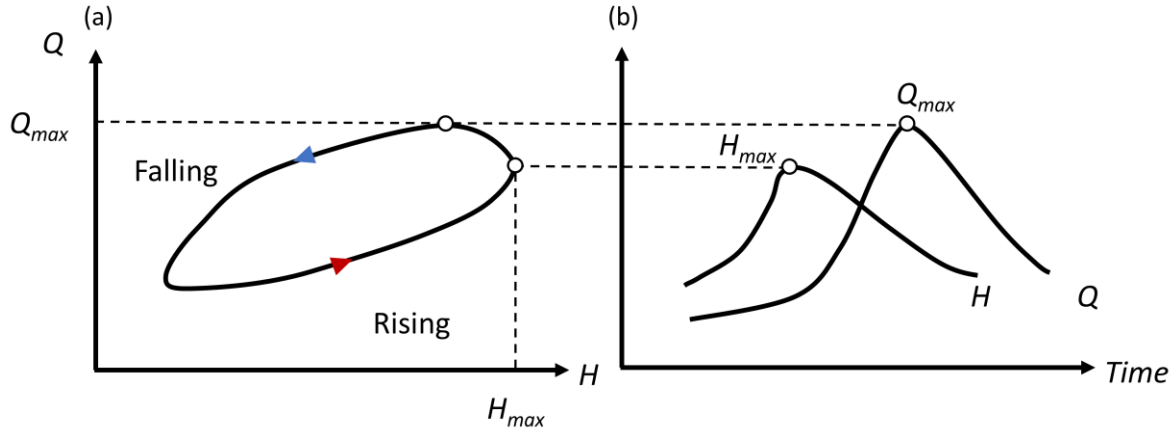

Figure 3. Illustration of the time-lag effect between water level and flow rate. (**a**) Hysteresis curve (H–Q curve) showing the dynamic relationship between water level and flow rate, with the area reflecting the time-lag effect; (**b**) hydrological process lines demonstrating the asynchrony between flow rate and water level. Note: The red arrow indicates the rising phase of the flow process, while the blue arrow represents the falling phase.

3. Results

3.1. Functionality and Independent Impact of Green Infrastructure

Green infrastructure significantly reduces peak runoff, alleviates network load, and enhances the system's lag effect by increasing permeability. Figure 4 illustrates the impact of green infrastructure on drainage network performance under varying permeability conditions (IAR = 40%, 51%, 65%).

(1) Peak Runoff and Pipe Load Reduction

Figure 4a shows that under high permeability conditions (IAR = 40%), the reduction of peak runoff is most significant during short recurrence intervals (P = 5), with a reduction rate exceeding 20%, which is notably higher than the approximately 13% observed under medium permeability conditions (IAR = 51%). However, as the recurrence interval increases (P = 1000), the reduction rate gradually decreases and stabilizes, with IAR = 40% stabilizing at 15% and IAR = 51% dropping to 7%. Similarly, Figure 4b depicts the reduction in average pipe load. For short recurrence intervals (P = 5), the reduction rate under high permeability (IAR = 40%) reaches 6.5%, far exceeding the 3.2% achieved under medium permeability (IAR = 51%). As the recurrence interval increases, the reduction in pipe load stabilizes at approximately 5.5% for IAR = 40% and 2.8% for IAR = 51%.

(2) Water Level–Flow Rate Relationship

Figure 4c,d present the water level–flow rate relationships for nodes and pipes under a 50-year recurrence interval (P = 50). Under high permeability conditions (IAR = 40%), the maximum flow rates for both nodes and pipes are significantly lower than those under medium and low permeability conditions (IAR = 51%, 65%). For instance, when node water levels approach full-pipe status (depth ~0.8 m), the flow rate under IAR = 40% is approximately 0.55 m^3/s, whereas under IAR = 65%, it reaches 0.7 m^3/s. Similarly, when pipe water levels approach full-pipe status, the flow rate under IAR = 40% is 0.35 m^3/s, substantially lower than the 0.45 m^3/s observed under IAR = 65%. These results highlight the peak reduction capability of green infrastructure.

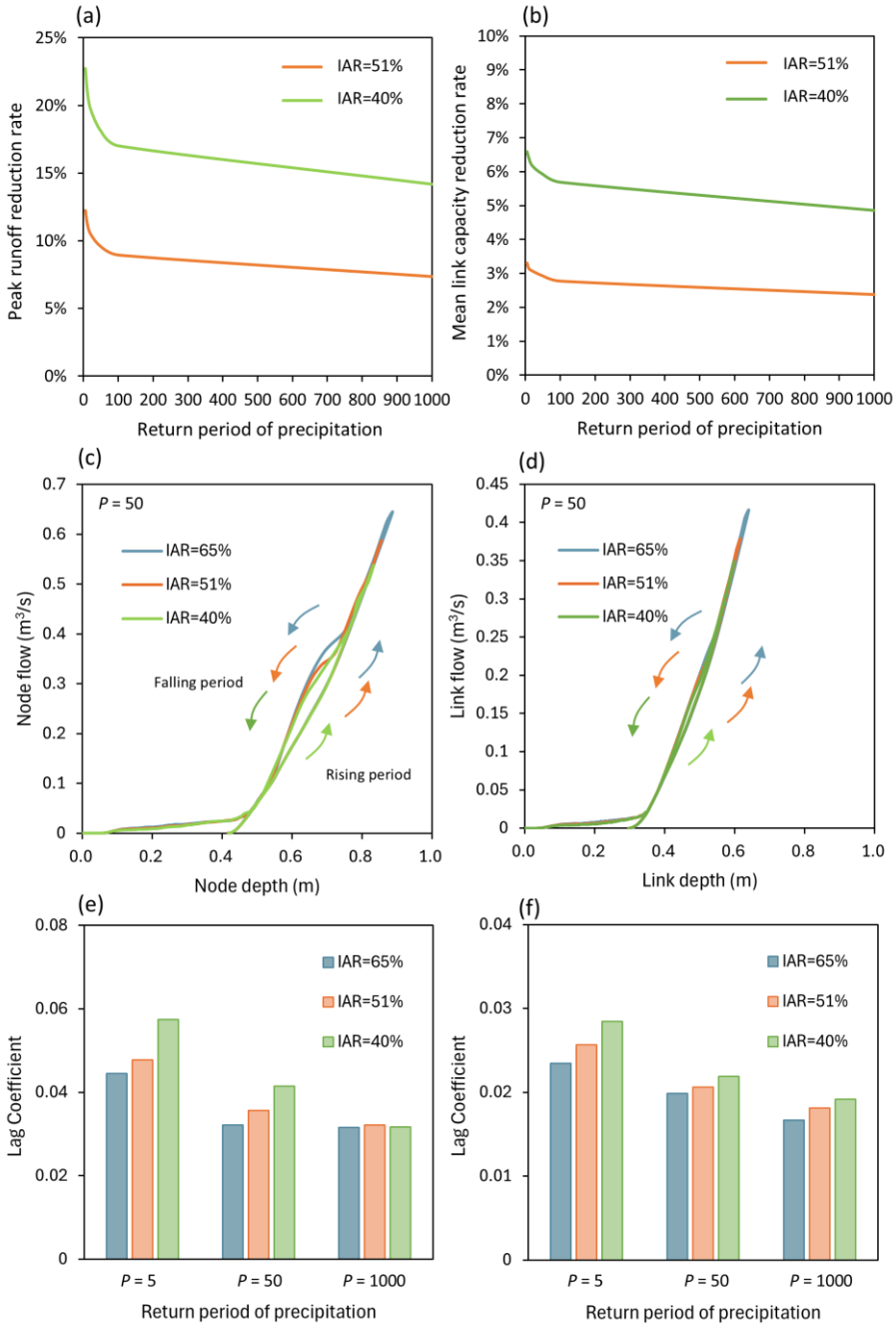

Figure 4. Impact of green infrastructure on drainage network performance under varying permeability conditions. (**a**) Peak runoff reduction rates under different recurrence intervals (relative to IAR = 65% baseline); (**b**) average pipe load reduction rates under different recurrence intervals (relative to IAR = 65% baseline); (**c**) hysteresis curves for node water level–flow rate relationships (P = 50); (**d**) hysteresis curves for pipe water level–flow rate relationships (P = 50); (**e**) node-lag coefficients under different recurrence intervals; (**f**) pipe-lag coefficients under different recurrence intervals. Note: The upward arrow denotes the rising phase of the flow process, whereas the downward arrow indicates the falling phase.

(3) Lag Effect

Figure 4e,f show the variations in lag coefficients for nodes and pipes under different rainfall recurrence intervals (P = 5, P = 50, P = 1000). A larger lag coefficient indicates a stronger ability of the system to reduce peak runoff and delay drainage. At the node level, high permeability conditions (IAR = 40%) exhibit significantly higher lag coefficients across

all recurrence intervals compared to medium and low permeability conditions (IAR = 51%, 65%). For example, under $P = 5$ conditions, the node-lag coefficient for IAR = 40% is 0.06, while for IAR = 65%, it is only 0.04. As rainfall intensity increases, the lag coefficient decreases; however, under extreme rainfall scenarios ($P = 1000$), differences in lag coefficients across permeability conditions become negligible. The lag effect for pipes follows a similar trend to nodes but is generally weaker, indicating a relatively lower peak reduction and lag capability.

In summary, the effectiveness of green infrastructure in reducing peak runoff, alleviating pipe network loads, and enhancing lag effects is influenced by both rainfall conditions and permeability levels. Under high permeability conditions, green infrastructure performs exceptionally well in small-to-medium rainfall scenarios, but its impact diminishes under extreme rainfall conditions.

3.2. Functionality and Independent Impact of Gray Infrastructure

Gray infrastructure significantly influences peak flow reduction, lag effects, and hydraulic stability through optimized pipe diameter (PD) design. Figure 5 illustrates the impact of gray infrastructure on node and pipe drainage performance under varying unit pipe diameter conditions (PD = 0.5 m, 1.0 m, 1.5 m). These pipe diameters were not selected based on specific design return periods but rather as test variables to analyze drainage performance trends across different rainfall intensities. This approach allows for a comparative assessment of how varying pipe sizes influence peak flow reduction and system stability under different storm conditions.

(1) Reduction Effect Analysis for Nodes and Pipes

Figure 5a,b illustrate the variation in reduction effectiveness for nodes and pipes across different rainfall return periods. Overall, nodes demonstrate superior reduction capabilities compared to pipes, and the improvement in reduction effectiveness due to increased pipe diameter is particularly significant under small-to-medium rainfall conditions. For short return periods ($P = 5$), the reduction rates for nodes with pipe diameters of 1.5 m and 1.0 m reach 75% to 82%. However, under extreme rainfall conditions ($P = 1000$), the reduction rates drop to 58% and 80%, respectively. For pipes, the reduction effectiveness is slightly lower but follows a similar trend to nodes. Under $P = 5$, the reduction rate for pipes with a diameter of 1.5 m is approximately 64%, compared to 36% for 1.0 m. For $P = 1000$, these reduction rates decrease to 49% and 15%, respectively. As rainfall intensity increases, the marginal improvement in reduction effectiveness due to increased pipe diameter diminishes.

(2) Water Level–Flow Rate Relationship

Figure 5c,d depict the water level–flow relationship under a 50-year return period ($P = 50$), revealing nonlinear characteristics. At the node level, the hysteresis curve under a pipe diameter of 0.5 m exhibits an "8" shape, indicating significant fluctuations in flow between the rising and falling stages, relatively strong lagging capacity, and poor hydraulic stability. As the pipe diameter increases, hydraulic stability gradually improves, and the peak flow also rises correspondingly. Specifically, for a pipe diameter of 1.5 m, the peak flow at nodes reaches 0.6 m^3/s, with the hysteresis curve's falling and rising segments nearly overlapping, signifying a notable reduction in lagging effects. At the pipe level, the hysteresis curve for a 0.5 m diameter also exhibits an "8" shape, with a relatively low peak flow of only 0.2 m^3/s. In contrast, for a 1.5 m pipe diameter, the peak flow significantly increases to approximately 0.4 m^3/s, and the curve nearly becomes a straight line, indicating a marked reduction in response delay to rainfall. This phenomenon suggests that larger pipe diameters enhance the drainage capacity of the system but weaken its lagging characteristics.

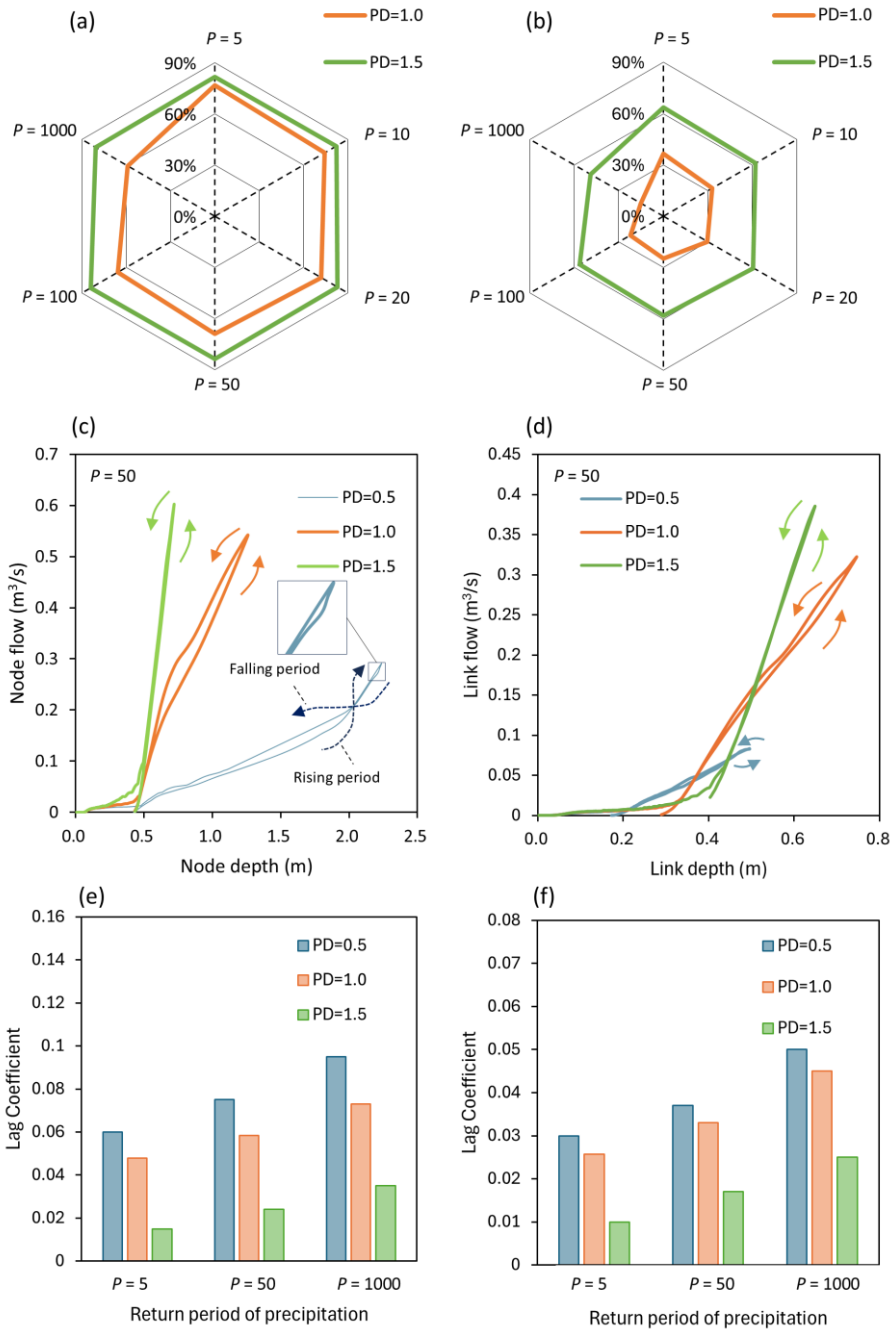

Figure 5. Impact of gray infrastructure on node and pipe drainage performance under different pipe diameters (PDs). (**a**) Node reduction in pipe load under different recurrence intervals; (**b**) pipe reduction in pipe load under different recurrence intervals; (**c**) hysteresis curves for node water level–flow rate relationships (P = 50); (**d**) hysteresis curves for pipe water level–flow rate relationships (P = 50); (**e**) hysteresis curve area (lag coefficient) for nodes under different recurrence intervals; (**f**) hysteresis curve area (lag coefficient) for pipes under different recurrence intervals. Note: The upward arrow denotes the rising phase of the flow process, whereas the downward arrow indicates the falling phase.

(3) Lag Effect Analysis

Figure 5e,f show the variation in lag effects for nodes and pipes, as reflected by the hysteresis curve area. The results indicate that nodes generally exhibit stronger lag effects than pipes. Lag effects decrease as rainfall recurrence intervals increase, with the hysteresis curve area shrinking significantly under extreme rainfall conditions (P = 1000). Under different pipe diameter conditions, PD = 0.5 m exhibits the most pronounced lag effects, with the largest

hysteresis curve areas for both nodes and pipes, especially under small-to-medium rainfall conditions (P = 5 and P = 50). PD = 1.0 m shows moderate lag effects, while PD = 1.5 m exhibits the weakest lag effects, with almost no lag observed under extreme rainfall scenarios (P = 1000). These findings indicate that smaller pipe diameters (PD = 0.5 m) offer stronger peak reduction and lag effects but have relatively low drainage efficiency. In contrast, larger pipe diameters (PD = 1.5 m) significantly enhance drainage capacity, making them more suitable for high-intensity rainfall events, though they may increase downstream drainage pressure.

In summary, optimizing pipe diameters in gray infrastructure has a significant impact on drainage system performance. Smaller pipe diameters (PD = 0.5 m and PD = 1.0 m) are well suited for small-to-medium rainfall scenarios, providing effective peak reduction and lag effects to alleviate drainage pressure. Larger pipe diameters (PD = 1.5 m) are more suitable for high-intensity rainfall events, enhancing drainage capacity to address extreme rainfall but potentially increasing downstream drainage pressure.

3.3. Functionality and Independent Impact of Blue Infrastructure

Blue infrastructure significantly influences peak reduction, lag effects, and hydraulic stability by adjusting the outlet water level. Figure 6 illustrates the specific effects of blue infrastructure on the hydraulic performance of nodes and pipes under different outlet water levels (WL = 7.5 m, WL = 7.0 m, WL = 6.5 m).

(1) Peak Reduction for Nodes and Pipes

As shown in Figure 6a,b, lowering the outlet water level enhances the reduction for both nodes and pipes, though the effectiveness decreases as the rainfall recurrence interval increases. At WL = 6.5 m, the reduction rate for nodes reaches approximately 10% for P = 5 and 8% for P = 10 but declines to about 2% for P = 1000. Under WL = 7.0 m, the reduction rate is significantly lower, achieving only 5% for P = 5 and negligible effects for P = 1000. For pipes, a similar trend is observed, but the reduction effect is less pronounced than for nodes. At WL = 6.5 m, the reduction rates are 8% for P = 5 and 6% for P = 10, dropping to less than 2% for P = 1000. When WL = 7.0 m, the reduction rate for P = 5 is approximately 4%, and it approaches zero for P = 1000.

(2) Water Level–Flow Rate Relationship

Figure 6c,d present the water level–flow rate relationships for nodes and pipes under a 50-year recurrence interval (P = 50), highlighting the effects of outlet water levels. At the node level (Figure 6c), reducing the outlet water level gradually decreases the peak water level, while changes in peak flow rate are insignificant. Specifically, under WL = 7.5 m, the peak water level is relatively high (approximately 1.26 m), with the hysteresis curve leaning to the right. When the outlet water level is reduced to WL = 7.0 m, the peak water level decreases to approximately 1.2 m, and the curve shifts left. Under WL = 6.5 m, the peak water level further drops to 1.16 m, with the curve shifting further left. At the pipe level (Figure 6d), the trends are similar to those observed at the node level, but changes in peak flow and lag effects are less pronounced. While the water level decreases slightly with lower outlet water levels, the curve shape only changes modestly. Overall, the outlet water level reduction has a more significant impact on the hydraulic conditions of nodes than on pipes.

(3) Lag Effect

Figure 6e,f show the variations in lag coefficients for nodes and pipes under different rainfall recurrence intervals. Nodes generally exhibit stronger lag effects than pipes, with lag effects increasing substantially with longer recurrence intervals. At the node level (Figure 6e), under WL = 7.5 m, the lag coefficients for P = 5, P = 50, and P = 1000 are approximately 0.06, 0.08, and 0.10, respectively. When the outlet water level is reduced to WL = 7.0 m, the coefficients decrease to approximately 0.05, 0.07, and 0.08. Under

WL = 6.5 m, they further decrease to approximately 0.04, 0.06, and 0.07. At the pipe level (Figure 6f), the lag effects are slightly weaker than at the node level but follow a similar trend. Under WL = 7.5 m, the lag coefficients for P = 5, P = 50, and P = 1000 are approximately 0.03, 0.04, and 0.07, respectively. These values decrease to 0.025, 0.035, and 0.06 under WL = 7.0 m and further to 0.02, 0.03, and 0.05 under WL = 6.5 m. These findings indicate that lowering the outlet water level significantly reduces lag effects for both nodes and pipes, with the impact being more pronounced for nodes.

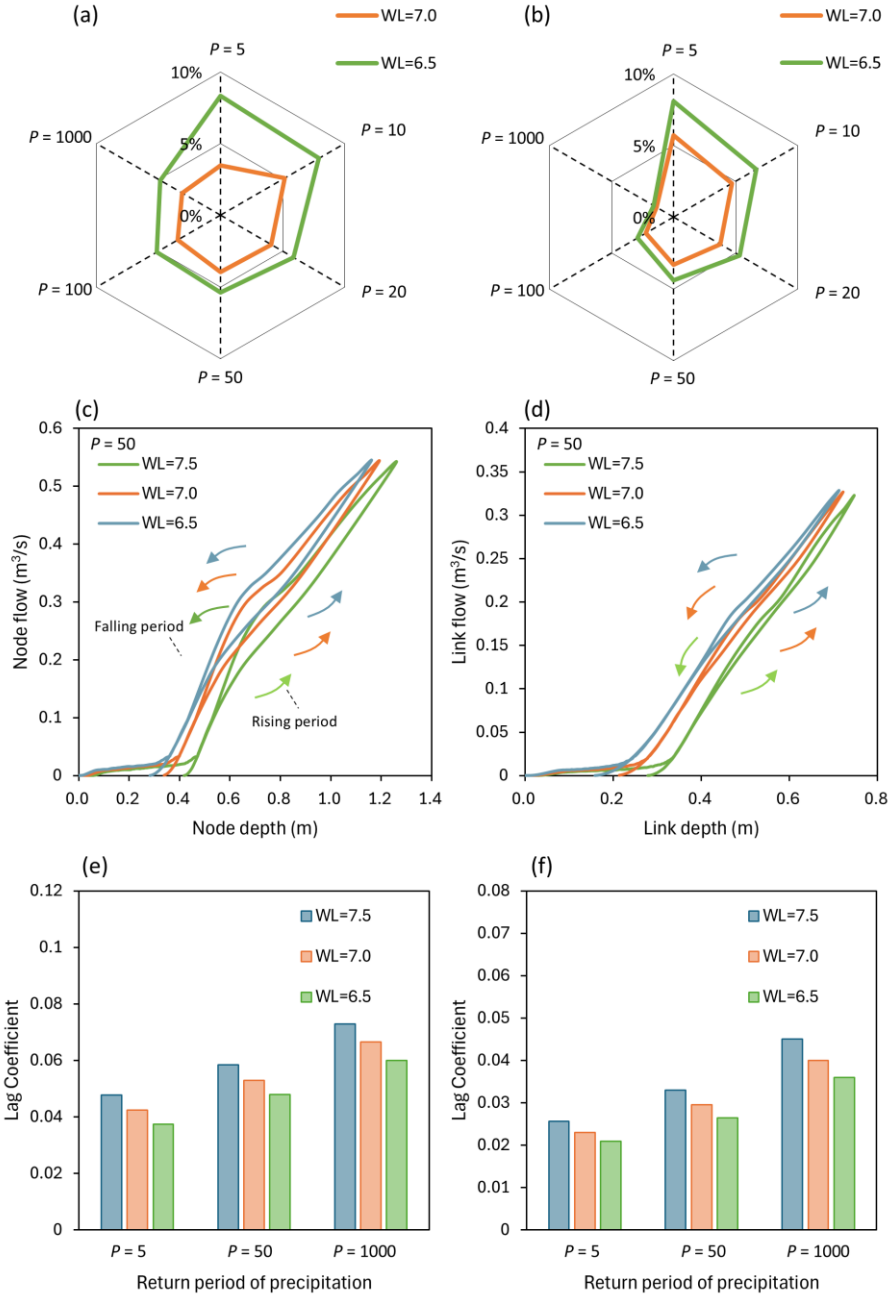

Figure 6. Effects of blue infrastructure on hydraulic characteristics of nodes and pipes under different outlet water levels (WLs). (**a**) Node pipe load reduction rates under different rainfall recurrence intervals; (**b**) pipe load reduction rates under different rainfall recurrence intervals; (**c**) node water level–flow rate hysteresis curves (P = 50); (**d**) pipe water level–flow rate hysteresis curves (P = 50); (**e**) node-lag coefficients under different rainfall recurrence intervals; (**f**) pipe-lag coefficients under different rainfall recurrence intervals. Note: The upward arrow denotes the rising phase of the flow process, whereas the downward arrow indicates the falling phase.

In summary, blue infrastructure enhances the drainage capacity of nodes and pipes by lowering the outlet water level while effectively reducing lag effects. For pipe load reduction, nodes consistently outperform pipes, with WL = 6.5 m showing the most significant effects, particularly under short recurrence intervals. In controlling lag effects, lowering the outlet water level has a more substantial impact on nodes, suggesting that nodes are more sensitive to flow lag effects. Compared to green infrastructure, which improves peak reduction and lag effects by optimizing permeability, blue infrastructure directly enhances drainage capacity and reduces lag effects through outlet water level regulation.

4. Discussion

4.1. Impact of Three Types of Infrastructure on the Hysteresis Curve

The hysteresis curve dynamically illustrates the relationship between the water level and flow rate, providing an intuitive reflection of the drainage system's peak reduction capacity, drainage efficiency, and lag effects. The results indicate significant differences in how green, gray, and blue infrastructures impact the hysteresis curve across three scenarios: past (pre-modification), present (initial modification), and future (future planning). These differences highlight the functional design focus and optimization trajectories unique to each type of infrastructure. However, the proposed scenarios do not incorporate modifications to the existing retention facilities, which could significantly influence hysteresis curve characteristics and lag effects. Retention basins play a crucial role in temporarily storing excess runoff, mitigating peak flow, and regulating system-wide drainage responses. Changes in their storage capacity or operational strategies could alter the overall system dynamics, potentially impacting the optimization pathways for green, gray, and blue infrastructure integration. Future studies should consider incorporating retention facility modifications to evaluate their synergistic effects on drainage performance.

(1) Green Infrastructure

In the past (pre-modification) scenario, the hysteresis curve is narrow with a notably reduced area, reflecting weaker peak reduction and lag regulation capacities. This limitation likely stems from the early design focus on localized runoff control rather than integrated regulation. In the present (initial modification) scenario, the area of the hysteresis curve increases slightly, and the curve shape becomes more symmetrical, indicating a balance between peak reduction capacity and drainage efficiency. In the future (future planning) scenario, green infrastructure significantly widens the horizontal width of the hysteresis curve and reduces its vertical height (Figure 7a), thereby extending the lag time. This improvement is attributed to enhanced core functionalities such as rainwater infiltration, storage, and detention.

(2) Gray Infrastructure

In the past (pre-modification) scenario, the hysteresis curve area is large and complex, occasionally exhibiting dual-loop structures. This reflects inconsistencies in peak reduction and lag regulation, potentially leading to reduced drainage efficiency and prolonged lag time. In the present (initial modification) scenario, the hysteresis curve area decreases slightly, and the shape becomes more symmetrical, suggesting improved drainage efficiency and a minor enhancement in peak reduction. In the future (future planning) scenario, gray infrastructure optimizes pipe network design and enhances drainage efficiency, compressing the horizontal width of the hysteresis curve while increasing its vertical height (Figure 7b). This signifies a marked improvement in the ability to rapidly convey flow, albeit with limited peak reduction and lag regulation effects.

(3) Blue Infrastructure

In the past (pre-modification) scenario, the area of the hysteresis curve is relatively large, indicating a less efficient regulation of peak flow. In the present (initial modification) scenario, blue infrastructure begins to show improved regulation capabilities, balancing peak reduction and rapid drainage. In the future (future planning) scenario, blue infrastructure significantly compresses the horizontal width of the hysteresis curve (Figure 7c), reducing lag effects while maintaining high drainage efficiency and peak reduction capacity.

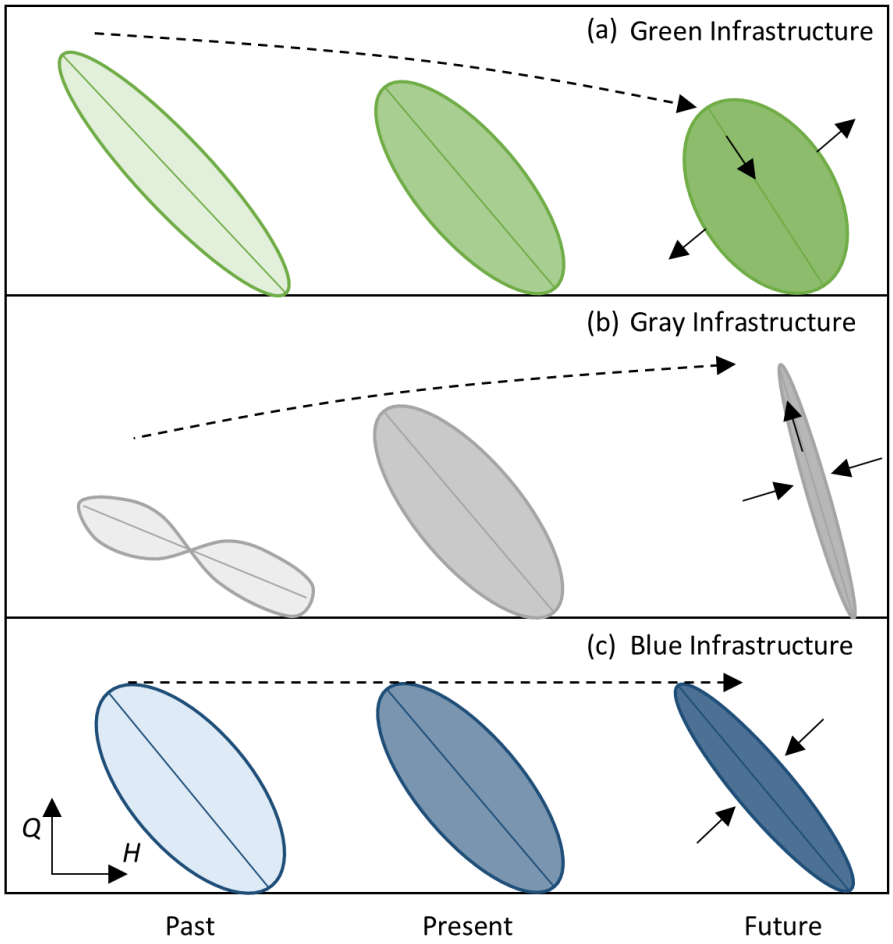

Figure 7. Impact of green, gray, and blue infrastructures on the hysteresis curve across scenarios. (**a**) Green infrastructure-induced changes in hysteresis curve morphology; (**b**) Gray infrastructure-induced changes in hysteresis curve morphology; (**c**) Blue infrastructure-induced changes in hysteresis curve morphology. Note: The solid arrows indicate the direction of hysteresis curve changes over time, while the dashed arrows represent the overall evolutionary trend of the infrastructure across different periods.

The unique functional characteristics of each type of infrastructure are reflected in their influence on the hysteresis curve. Green infrastructure excels in peak reduction and lag regulation by widening the horizontal and shortening the vertical dimensions of the curve, making it well suited for small-to-medium rainfall conditions. Gray infrastructure focuses on rapid drainage, compressing the horizontal width of the curve, but with limited impact on peak reduction and lag regulation. Blue infrastructure reduces lag effects and enhances drainage efficiency by compressing the curve horizontally, making it ideal for high-intensity rainfall scenarios. The combined optimization of these infrastructures provides an effective balance between drainage efficiency and regulation capabilities.

4.2. Differences and Mechanisms of Peak Reduction and Drainage Capacity

Peak reduction and drainage capacity are critical indicators for evaluating the performance of a drainage system. The mechanisms and applicable scenarios vary significantly among different types of infrastructure.

(1) Green Infrastructure

Green infrastructure primarily achieves peak reduction through permeability optimization and pipe diameter adjustments, with peak reduction being particularly prominent under small-to-medium rainfall conditions. The findings reveal that smaller pipe diameters effectively reduce peak flow and extend lag time, whereas larger pipe diameters enhance drainage capacity but weaken peak reduction. This balance makes green infrastructure suitable for scenarios with high peak reduction demands as its distributed optimization of nodes achieves synergistic effects in peak reduction and lag regulation.

(2) Gray Infrastructure

Focused on rapid drainage, gray infrastructure exhibits relatively weak peak reduction capabilities. Its impact relies mainly on the efficiency of pipe networks and pumping stations to mitigate localized ponding and indirectly control peak flow. In the future planning scenario, the role of gray infrastructure in peak reduction diminishes further, functioning primarily as a backbone to support the synergistic regulation of green and blue infrastructure. Its high-efficiency drainage characteristics ensure that urban drainage systems can swiftly convey runoff under intense rainfall conditions in high-density urban areas, preventing widespread flooding.

(3) Blue Infrastructure

Blue infrastructure achieves comprehensive flow regulation by adjusting outlet water levels, with peak reduction being particularly pronounced under high-intensity rainfall conditions. Lowering outlet water levels significantly enhances peak reduction for nodes and pipes, especially under extreme rainfall scenarios (P = 1000), where blue infrastructure makes a substantial contribution to peak flow mitigation. By strengthening overall hydraulic regulation, blue infrastructure becomes an essential tool for addressing rapid drainage and peak reduction needs, making it especially suitable for flood control in extreme rainfall events.

4.3. Functional Complementarity and Optimization Pathways of the Three Types of Infrastructure

Green, gray, and blue infrastructures exhibit distinct yet complementary roles in urban drainage systems, making their strategic integration essential for effective flood management. While green infrastructure focuses on source control and decentralized runoff management, gray infrastructure serves as the backbone for rapid drainage, and blue infrastructure regulates hydraulic conditions and peak attenuation.

To optimize drainage system performance, future urban planning should emphasize an adaptive, hybrid approach that leverages the strengths of each infrastructure type. Recent studies indicate that integrating green, hybrid, and gray infrastructure enhances disaster risk reduction and urban resilience [31], while a decentralized blue–green–gray simulation–optimization framework has demonstrated its effectiveness in improving drainage efficiency [32]. This suggests that hybrid solutions incorporating real-time water level regulation, pipe network optimization, and enhanced permeability strategies can significantly improve urban flood resilience.

Strategic Optimization Pathways: For small-to-medium rainfall scenarios, green infrastructure should be prioritized for its peak reduction and lag extension capabilities, alleviating system load while promoting infiltration and retention. For high-intensity and

extreme rainfall conditions, blue infrastructure should be optimized for real-time hydraulic control, while gray infrastructure ensures efficient flow conveyance and structural drainage stability. A coordinated integration of these three infrastructure types can enhance system adaptability to variable rainfall conditions, reduce urban flooding risks, and improve long-term drainage resilience.

5. Conclusions

This study systematically analyzed the peak reduction capacity, lag effects, and drainage efficiency of green, gray, and blue infrastructures in urban drainage systems. Using hysteresis curve morphology across different scenarios, it revealed functional differences and collaborative optimization pathways among the three types of infrastructure. The main conclusions are as follows:

(1) By enhancing permeability and optimizing infiltration capabilities, green infrastructure demonstrates exceptional peak reduction and lag regulation in small-to-medium rainfall conditions. In future planning scenarios, it significantly widens the horizontal width and shortens the vertical height of the hysteresis curve, extending lag time and highlighting its comprehensive advantages in mitigating peak flow and distributing runoff. However, its peak reduction effect diminishes in extreme rainfall scenarios, indicating that its primary functionality lies in the integrated regulation of small-to-medium rainfall events.

(2) Gray infrastructure supports the core functionality of the drainage system by optimizing pipe diameters and improving drainage efficiency. The study found that large pipe diameters significantly enhance drainage efficiency but have relatively weaker peak reduction effects. Its lag effect diminishes further in future planning scenarios, underscoring its role in rapidly conveying flow. In high-density urban areas, gray infrastructure's efficient drainage capabilities are critical for addressing heavy rainfall and localized flooding. However, it requires integration with other infrastructure for effective peak reduction and lag regulation.

(3) Through flexible water level regulation, blue infrastructure exhibits remarkable peak reduction and rapid drainage capabilities under high-intensity and extreme rainfall conditions. By lowering outlet water levels, it significantly compresses the horizontal width of the hysteresis curve, reduces lag effects, and maintains high drainage efficiency. Its overall hydraulic regulation capabilities make it a critical tool for extreme rainfall management, acting as a stabilizer and flow regulator within the system.

(4) The functional differences among the three types of infrastructure provide essential guidance for optimizing drainage system design. Green infrastructure is well suited for small-to-medium rainfall conditions, enhancing system resilience through retention and decentralized peak reduction. Gray infrastructure serves as the system's backbone, addressing heavy rainfall drainage needs in high-density urban areas. Blue infrastructure provides exceptional peak reduction and rapid drainage capabilities under high-intensity rainfall scenarios through overall hydraulic regulation. Future drainage systems should capitalize on the complementary functions of these infrastructures to enable dynamic regulation under various rainfall conditions, meeting diverse urban flood management and drainage needs.

Author Contributions: All authors contributed to the research conception and design. The material preparation, data collection, and analysis were performed by Y.Y. (Yang Yu), Y.Y. (Yi Yao), D.L. and C.L. Y.Y. (Yang Yu) wrote the first draft of the manuscript, and all authors commented on previous versions of the manuscript. All authors have read and agreed to the published version of the manuscript.

Funding: This research was funded by the Key R&D Program of China (2022YFC3004400), National Natural Science Foundation of China (52209170).

Data Availability Statement: The original contributions presented in this study are included in the article. Further inquiries can be directed to the corresponding author.

Conflicts of Interest: The authors declare that there are no conflicts of interest.

References

1. Schmitt, T.; Thomas, M.; Ettrich, N. Analysis and Modeling of Flooding in Urban Drainage Systems. *J. Hydrol.* **2004**, *299*, 300–311. [CrossRef]
2. Dong, X.; Guo, H.; Zeng, S. Enhancing Future Resilience in Urban Drainage System: Green versus Grey Infrastructure. *Water Res.* **2017**, *124*, 280–289. [CrossRef]
3. Zhang, Q.; Wu, Z.; Cao, Z.; Guo, G.; Zhang, H.; Li, C.; Tarolli, P. How to Develop Site-Specific Waterlogging Mitigation Strategies? Understanding the Spatial Heterogeneous Driving Forces of Urban Waterlogging. *J. Clean. Prod.* **2023**, *422*, 138595. [CrossRef]
4. Roy, S.; Bose, A.; Singha, N.; Basak, D.; Chowdhury, I.R. Urban Waterlogging Risk as an Undervalued Environmental Challenge: An Integrated MCDA-GIS Based Modeling Approach. *Environ. Chall.* **2021**, *4*, 100194. [CrossRef]
5. Todeschini, S. Trends in Long Daily Rainfall Series of Lombardia (Northern Italy) Affecting Urban Stormwater Control. *Int. J. Climatol.* **2012**, *32*, 900–919. [CrossRef]
6. Cameron, R.W.F.; Blanuša, T.; Taylor, J.E.; Salisbury, A.; Halstead, A.J.; Henricot, B.; Thompson, K. The Domestic Garden—Its Contribution to Urban Green Infrastructure. *Urban For. Urban Green.* **2012**, *11*, 129–137. [CrossRef]
7. Sandstro¨m, U.G. Green Infrastructure Planning in Urban Sweden. *Plan. Pract. Res.* **2002**, *17*, 373–385. [CrossRef]
8. Tzoulas, K.; Korpela, K.; Venn, S.; Yli-Pelkonen, V.; Kaźmierczak, A.; Niemela, J.; James, P. Promoting Ecosystem and Human Health in Urban Areas Using Green Infrastructure: A Literature Review. *Landsc. Urban Plan.* **2007**, *81*, 167–178. [CrossRef]
9. Tian, J.; He, G. Optimization Design Method for Urban Sewage Collection Pipe Networks. *Water Sci. Technol.* **2020**, *81*, 1828–1839. [CrossRef] [PubMed]
10. Steele, J.C.; Mahoney, K.; Karovic, O.; Mays, L.W. Heuristic Optimization Model for the Optimal Layout and Pipe Design of Sewer Systems. *Water Resour. Manag.* **2016**, *30*, 1605–1620. [CrossRef]
11. Veerkamp, C.J.; Schipper, A.M.; Hedlund, K.; Lazarova, T.; Nordin, A.; Hanson, H.I. A Review of Studies Assessing Ecosystem Services Provided by Urban Green and Blue Infrastructure. *Ecosyst. Serv.* **2021**, *52*, 101367. [CrossRef]
12. Valente de Macedo, L.S.; Barda Picavet, M.E.; Puppim de Oliveira, J.A.; Shih, W.-Y. Urban Green and Blue Infrastructure: A Critical Analysis of Research on Developing Countries. *J. Clean. Prod.* **2021**, *313*, 127898. [CrossRef]
13. Muste, M.; Kim, D.; Kim, K. A Flood-Crest Forecast Prototype for River Floods Using Only in-Stream Measurements. *Commun. Earth Environ.* **2022**, *3*, 78. [CrossRef]
14. Di Baldassarre, G.; Montanari, A. Uncertainty in River Discharge Observations: A Quantitative Analysis. *Hydrol. Earth Syst. Sci.* **2009**, *13*, 913–921. [CrossRef]
15. Muste, M.; Lee, K.; Kim, D.; Bacotiu, C.; Oliveros, M.R.; Cheng, Z.; Quintero, F. Revisiting Hysteresis of Flow Variables in Monitoring Unsteady Streamflows. *J. Hydraul. Res.* **2020**, *58*, 867–887. [CrossRef]
16. Liu, W.; Chen, W.; Peng, C. Assessing the Effectiveness of Green Infrastructures on Urban Flooding Reduction: A Community Scale Study. *Ecol. Model.* **2014**, *291*, 6–14. [CrossRef]
17. Wang, Z.; Li, Z.; Wang, Y.; Zheng, X.; Deng, X. Building Green Infrastructure for Mitigating Urban Flood Risk in Beijing, China. *Urban For. Urban Green.* **2024**, *93*, 128218. [CrossRef]
18. Zhen, M.A.; Xia, Y.; Li, H.; Han, B.; Yu, X.; Zhou, Y.; Wang, Y.; Guo, X.; Li, H.; Pei, Y. Analysis of Natural Resources and Environment Eco-Geological Conditions in the Xiong'an New Area. *Geol. China* **2021**, *48*, 677–696. [CrossRef]
19. Ouyang, Q.; Pan, J. Evaluating Land Use and Ecological Patterns in Xiong'an New Area of China with Machine Learning Methodology. *Remote Sens.* **2024**, *16*, 495. [CrossRef]
20. Xu, H.; Shi, T.; Wang, M.; Fang, C.; Lin, Z. Predicting Effect of Forthcoming Population Growth–Induced Impervious Surface Increase on Regional Thermal Environment: Xiong'an New Area, North China. *Build. Environ.* **2018**, *136*, 98–106. [CrossRef]
21. Wang, Y.; Zhang, X.; Tang, Q.; Mu, M.; Zhang, C.; Lv, A.; Jia, S. Assessing Flood Risk in Baiyangdian Lake Area in a Changing Climate Using an Integrated Hydrological-Hydrodynamic Modelling. *Hydrol. Sci. J.* **2019**, *64*, 2006–2014. [CrossRef]
22. Zou, Y.; Chen, Z.; Zhong, N.; Zhao, W. Urban Planning as a Way to Pursue Quality-Oriented Urbanization: Anatomy of the Urban Planning of Xiong'an New Area, China. *J. Urban Aff.* **2023**, *45*, 1418–1433. [CrossRef]
23. Si, L.; Zhao, L.; Chen, Z.; Chen, X.; Zhao, T.; Xie, W.; Wang, B.; Wang, Y. Impact-Based Critical Areal Rainfall for Early Flood Warning: A Case Study of Zhulong River Watershed in the Upper Reaches of the Xiong'an New Area. *Atmosphere* **2023**, *14*, 113. [CrossRef]

24. Wu, F.; Guo, N.; Kumar, P.; Niu, L. Scenario-based Extreme Flood Risk Analysis of Xiong'an New Area in Northern China. *J. Flood Risk Manag.* **2021**, *14*, e12707. [CrossRef]
25. Sun, W.; Sun, Y.; Li, X.; Wang, T.; Wang, Y.; Qiu, Q.; Deng, Z. Evaluation and Correction of GPM IMERG Precipitation Products over the Capital Circle in Northeast China at Multiple Spatiotemporal Scales. *Adv. Meteorol.* **2018**, *2018*, 4714173. [CrossRef]
26. Chen, X.; Xu, Y.; Li, T.; Wei, J.; Wu, J. Regional Rainfall Damage Functions to Estimate Direct Economic Losses in Rainstorms: A Case Study of the 2016 Extreme Rainfall Event in Hebei Province of China. *Int. J. Disaster Risk Sci.* **2024**, *15*, 508–520. [CrossRef]
27. Zhang, B.; Fan, Z.; Du, Z.; Zheng, J.; Luo, J.; Wang, N.; Wang, Q. A Geomorphological Regionalization Using the Upscaled DEM: The Beijing-Tianjin-Hebei Area, China Case Study. *Sci. Rep.* **2020**, *10*, 10532. [CrossRef]
28. Haizhou, T.; Graf, W.H. Friction in Unsteady Open-Channel Flow over Gravel Beds. *J. Hydraul. Res.* **1993**, *31*, 99–110. [CrossRef]
29. Gharari, S.; Razavi, S. A Review and Synthesis of Hysteresis in Hydrology and Hydrological Modeling: Memory, Path-Dependency, or Missing Physics? *J. Hydrol.* **2018**, *566*, 500–519. [CrossRef]
30. Tang, H.; Chen, K.; Yuan, S.; Xu, L.; Qiu, J.; Lin, Q.; Gualtieri, C. Effects of Tributary Inflows on Unsteady Flow Hysteresis and Hydrodynamics in the Mainstream. *Hydrol. Res.* **2024**, *55*, 815–833. [CrossRef]
31. Anderson, C.C.; Renaud, F.G.; Hanscomb, S.; Gonzalez-Ollauri, A. Green, Hybrid, or Grey Disaster Risk Reduction Measures: What Shapes Public Preferences for Nature-Based Solutions? *J. Environ. Manag.* **2022**, *310*, 114727. [CrossRef]
32. Bakhshipour, A.E.; Dittmer, U.; Haghighi, A.; Nowak, W. Hybrid Green-Blue-Gray Decentralized Urban Drainage Systems Design, a Simulation-Optimization Framework. *J. Environ. Manag.* **2019**, *249*, 109364. [CrossRef] [PubMed]

Disclaimer/Publisher's Note: The statements, opinions and data contained in all publications are solely those of the individual author(s) and contributor(s) and not of MDPI and/or the editor(s). MDPI and/or the editor(s) disclaim responsibility for any injury to people or property resulting from any ideas, methods, instructions or products referred to in the content.